Available online at www.sciencedirect.com
ScienceDirect
Ceramics International 37 (2011) 783–789
CERAMICS INTERNATIONAL
www.elsevier.com/locate/ceramint

TiAl/B_4C marine material—Fabrication, mechanical and corrosion properties

Weike Zhang [a,b], Lizhen Gao [b,*], Jian Li [a], Baoju Yang [a], Yansheng Yin [a,c,**]

[a] Institute of Materials Science and Engineering, Ocean University of China, Qingdao 266100, China
[b] School of Mechanical Engineering, University of Western Australia, 35 Stirling Highway, WA 6009, Australia
[c] Institute of Marine Materials Science and Engineering, Shanghai Maritime University, Shanghai 201306, China

Received 3 June 2010; received in revised form 2 September 2010; accepted 7 October 2010
Available online 17 November 2010

Abstract

A novel TiAl/B_4C intermetallic/ceramic matrix composite was fabricated by high energy ball milling followed by hot press sintering. The microstructure of TiAl/B_4C composite was studied and its mechanical properties and corrosion resistance behaviors were investigated. The bending strength and fracture toughness of the composite reached 437.3 MPa and 4.85 MPa $m^{1/2}$, respectively, i.e., much higher values than the monolithic phase B_4C. The potentiodynamic polarization measurements and electrochemical impedance spectroscopy results indicated the excellent corrosion resistance of such composite material.

Keywords: TiAl intermetallics; TiAl/B4C composite; Mechanical properties; Corrosion resistance; Electrochemical impedance spectroscopy

1. Introduction

The discovery of hydrothermal vent systems of diverse chemical and biological environment at depths between 1600 and 3000 m in the sea has stimulated new theories on life's origins [1]. However, research on these systems in deep sea is still challenging on multiple levels, such as extreme pressure, steep thermal and chemical gradients, abundant microorganisms and hydrothermal fluids highly concentrated in sulfide [2]. Therefore, light weight, high strength, excellent corrosion resistance and anti-adhesion advanced marine materials are needed for the exploration of the deep sea. A multitude of materials are vying to rule the deep seas. Steel, aluminum and composite materials are competing to be the material of choice, with each making waves depending on the craft under consideration [3]. Boron carbide (B_4C) ceramics, exhibiting excellent properties, such as ultrahigh hardness, high wear resistance and melting point, effective thermal conductivity, low density, good chemical inertness, corrosion resistance and neutron absorption capability, have been received much attraction for a variety of applications including light weight armor plating, blasting nozzles, mechanical seal faces, grinding and cutting tools [4,5]. However, the widespread applications of B_4C are restricted by its relatively low strength (200–300 MPa) and fracture toughness (2–3 MPa $m^{1/2}$) as well as poor sinterability [6]. Intermetallic compounds show the features of both metals and ceramics, and are increasingly receiving more and more attentions. The mechanical properties will be improved when the intermetallics are intercalated into B_4C and form composites. The heat resistance of the ceramic joints can also be improved if intermetallic compounds are used as strengthening layers or secondary phases in the ceramic joining. Therefore, in the present study, considering that the TiAl intermetallic compounds show good corrosion resistance in the sea and relatively high toughness compared with ceramics [7], B_4C ceramic matrix composites are fabricated via high energy milling and reactive hot press sintering with different contents of TiAl intermetallics serving as additives. The microstructures and mechanical properties of the TiAl/B_4C composites have been investigated as well. Particular attention is given to the corrosion resistance behavior of the composites under seawater conditions.

* Corresponding author. Tel.: +61 8 6488 4782; fax: +61 8 6488 1024.
** Corresponding author at: Institute of Materials Science and Engineering, Ocean University of China, Qingdao 266100, China.
Tel: +86 532 6678 1795; fax: +86 532 6678 3292.
E-mail addresses: lizhen@mech.uwa.edu.au (L. Gao), yys2006@ouc.edu.cn (Y. Yin).

0272-8842/$36.00
doi:10.1016/j.ceramint.2010.10.019

2. Experimental

TiAl intermetallic powders were prepared by mechanical alloying (MA) using Ti (99.5% in purity) and Al (99.5% in purity) powders (Ti/Al = 1, molar ratio) as starting materials in a planetary ball mill (zirconia lining) with ZrO_2 ball (8 mm in diameter, ball to powder mass ratio of 10:1) at room temperature. After being milled for 30 h, the B_4C powder was added and further milled for another 12 h. The dried powder mixtures were hot press sintered in graphite dies at 1700–1750 °C for 1 h under a pressure of 20 MPa in a vacuum atmosphere. A series of TiAl/B_4C composite samples (#1: 10 wt.%TiAl/B_4C; #2: 20 wt.%TiAl/B_4C; #3: 30 wt.%TiAl/B_4C; #4: 40 wt.%TiAl/B_4C) were made for mechanical and corrosion resistance studies.

The sintered samples were shaped in Φ60 mm disks, both faces of which were polished before the hardness was tested on a HRA tester (HD-187.5). Density of the specimen was measured by the Archimedes immersion technique. The disks (Φ60 mm) was cut into (a) 3 mm × 4 mm × 30 mm specimens for measuring the bending strength in digital tension and compression tester (LYS-50000) and (b) 2 mm × 4 mm × 30–40 mm specimens with a notch 2 mm in depth and 0.25 mm in width for measuring the fracture toughness (single-edge notched beam-SENB) over the same tester. Five specimens for each material were tested and the average value was obtained for analysis. Crystalline phase was identified by XRD (Rigaku, RINT-2000), using CuKα radiation at 40 kV and 30 mA. The morphology of fracture surface and phase distribution were investigated by Scanning Electron Microscopy (SEM, Hitachi S-2500) with the EDS system.

Prior to corrosion measurements, the samples were painted with epoxy resin, and a back lead was contacted by a silver paste, leaving an exposed area of 10 mm × 10 mm on the material surface. The front surface was polished using silicon carbide papers (from 400 to 1600 grade), then degreased with acetone, washed with distilled water and dried in air. The working cell was a standard three-electrode cell having a Pt net as a counter electrode and Hg/HgO (E_0 = +0.098 V/NHE) as reference electrode. Working solution was natural seawater at room temperature. Electrochemical impedance spectroscopy (EIS) was performed by IM6 electrochemical workstation. EIS measurements were performed in the frequency range between 10 MHz and 100 kHz with a sine-wave amplitude of 10 mV. The experimental EIS spectra were interpreted on the basis of equivalent electrical analogs using the Zview 2.0 program to obtain the fitting parameters. Polarization curves were recorded

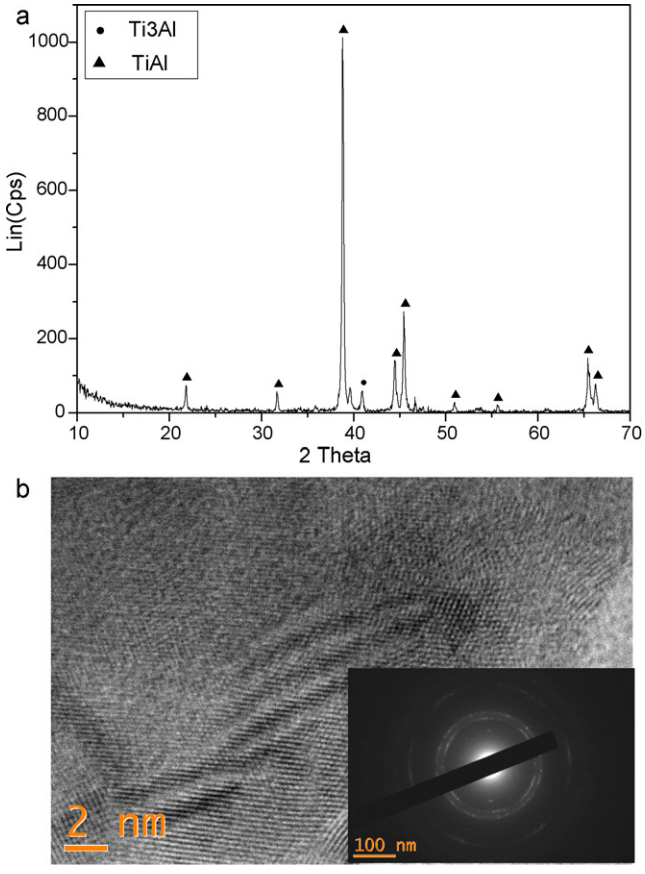

Fig. 1. (a) XRD pattern and (b) HRTEM image of TiAl intermetallic powder after ball milling.

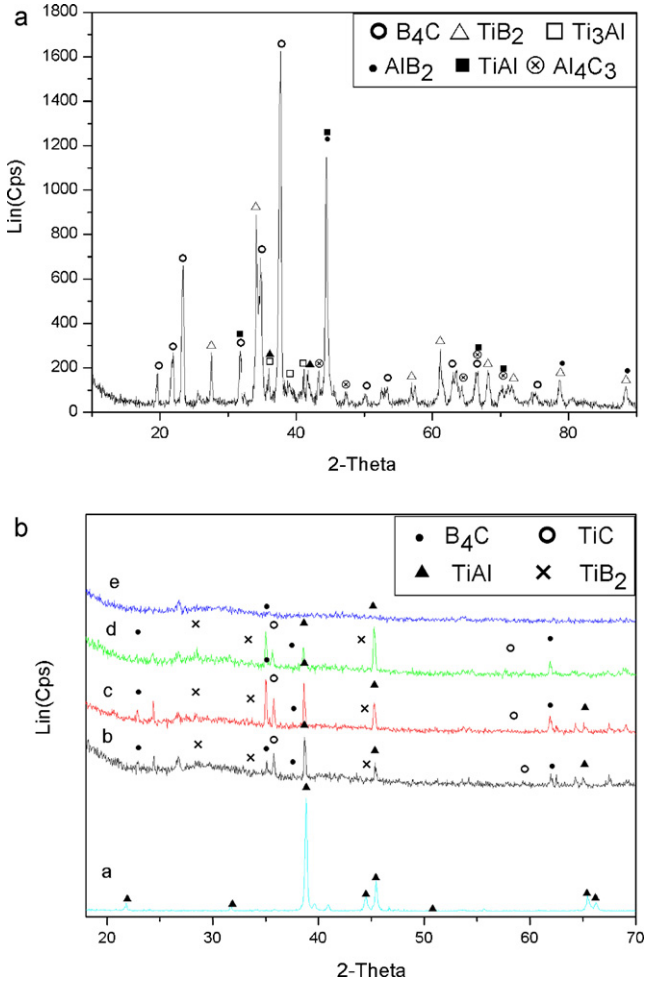

Fig. 2. XRD patterns of (a) 20 wt.%TiAl/B_4C after ball milling; (b) TiAl/B_4C after hot press sintering (a: TiAl intermetallic; b: 10 wt.%TiAl/B_4C; c: 20 wt.%TiAl/B_4C; d: 30 wt.%TiAl/B_4C; e: 40 wt.%TiAl/B_4C).

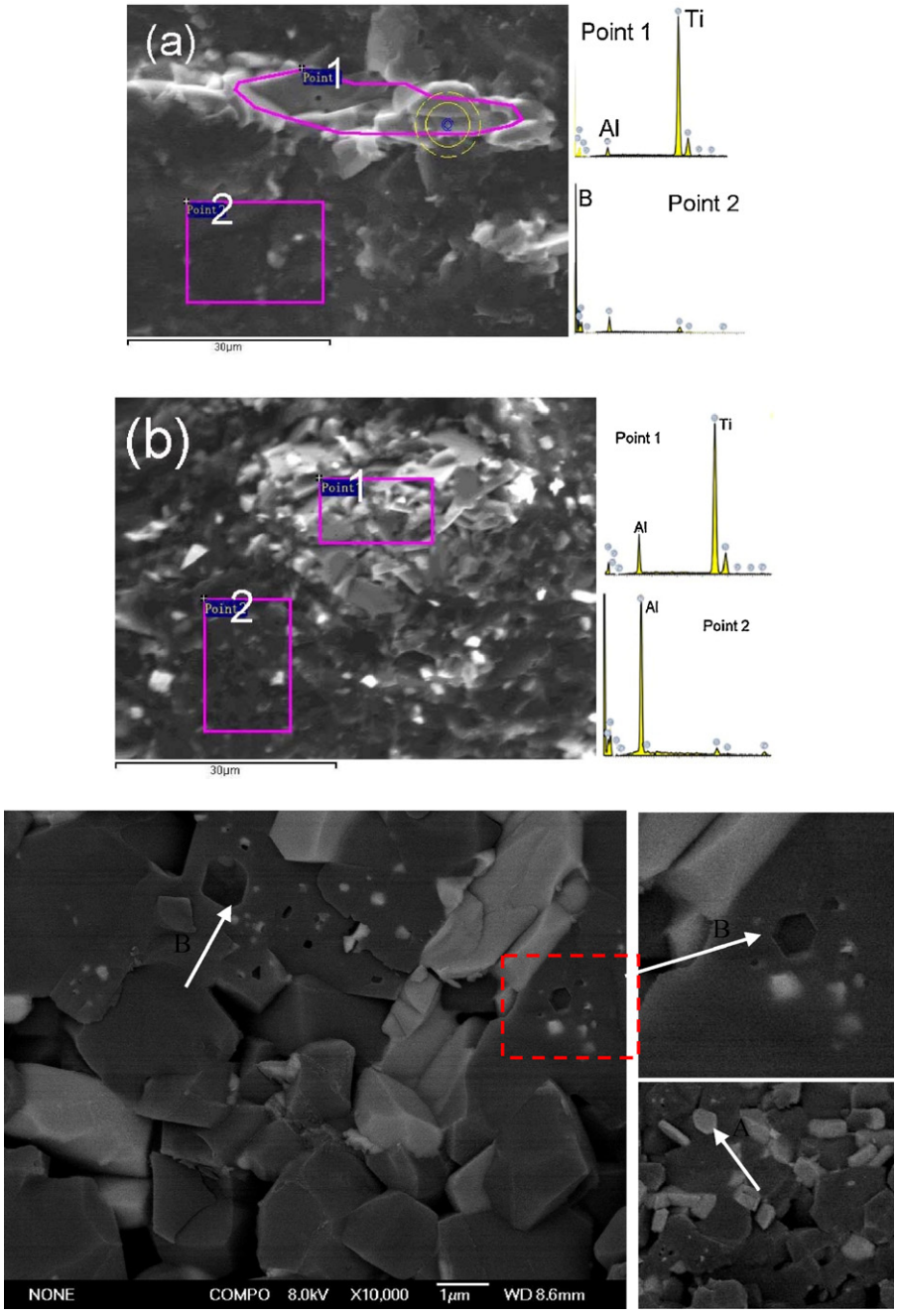

Fig. 3. SEM images and EDS spectra of (a) 20 wt.%TiAl/B_4C, (b) 40 wt.%TiAl/B_4C; (c) highlighting of point 2 in (a).

at a scan rate of 2 mV/s. All the potentials were referred to the saturated calomel electrode (SCE).

3. Results and discussion

3.1. Microstructure of the composites

During high-energy ball milling the powder particles are repeatedly flattened, cold welded, fractured and re-welded. Whenever two balls collide, some amount of powder is trapped in between them. The XRD patterns and HRTEM image of the Ti and Al mixture after mechanical alloying process are shown in Fig. 1a and b respectively. The results indicate the formation of TiAl intermetallic phase by diffusion of Al atoms into the Ti lattice as the main reaction product. As an example, the XRD pattern of the blended powders (#2: 20 wt.%TiAl/B_4C) after 30 h milling is shown in Fig. 2a. Apart from the B_4C and TiAl original phases, new phases, i.e., TiB_2, AlB_2, Al_4C_3 are detected, indicating the interaction between the TiAl and B_4C. The XRD patterns of samples with different proportions of TiAl after hot press sintering (Fig. 2b), shows the final products to be, as expected, B_4C, TiC, TiAl and TiB_2. The XRD pattern of the 40 wt.% TiAl (sample #4) shows very weak diffraction peaks, probably due to the TiAl liquid being in a glassy state (steep drop in cooling).The SEM images together with the EDS of sample #2 and sample #4 are shown in Fig. 3. For the

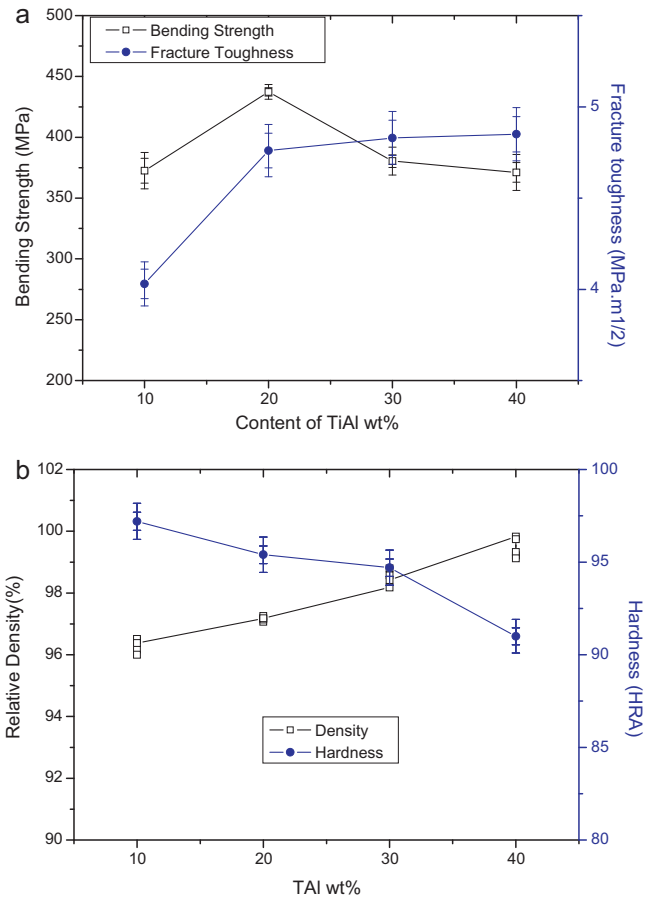

Fig. 4. Mechanical properties of TiAl/B_4C composites: (a) bending strength and fracture toughness; (b) relative density curve and hardness.

20 wt.% TiAl (sample #2), a sandwich structured composite is formed. The EDS spectrum indicates that the bright sandwich filling is predominantly TiAl (point 1), the sandwich skins being B_4C and other minor phase (point 2). When the TiAl amount was increased up to 40 wt.%, the TiAl is agglomerated into large lumps, leading to an unsatisfactory microstructure. The SEM image highlighting the dark part in Fig. 3a is shown in Fig. 3c. The sample exhibits laminated, rod-like and intragranular structures. These structures have a very positive effect for the mechanical properties of the samples. According to Zou et al. [8], TiB_2 crystallizes in a typical hexagonal prismatic or rectangular form [9] and TiC in a spherical or round shape [10].

3.2. Mechanical properties of TiAl/B_4C marine materials

Fracture toughness and bending strength of the composite samples are shown in Fig. 4a. The measurement errors are at around 3–5%. The fracture toughness for 20 wt.% TiAl is much higher than for 10 wt.% TiAl, nevertheless higher amount of TiAl do not show any significant effect. The bending strength peaked at 20 wt.% TiAl. These results indicate that the sandwich structured TiAl intercalation is the most appropriate for both the bending strength (437.3 MPa) and the fracture toughness (4.85 MP $m^{1/2}$). For samples #4, the TiAl alloys are agglomerated in dumpling so that their bending strength drastically declines but the fracture toughness is similar to sample #2.

Fig. 4b shows the relative density and hardness curves of the composite with different contents of Ti and Al. The

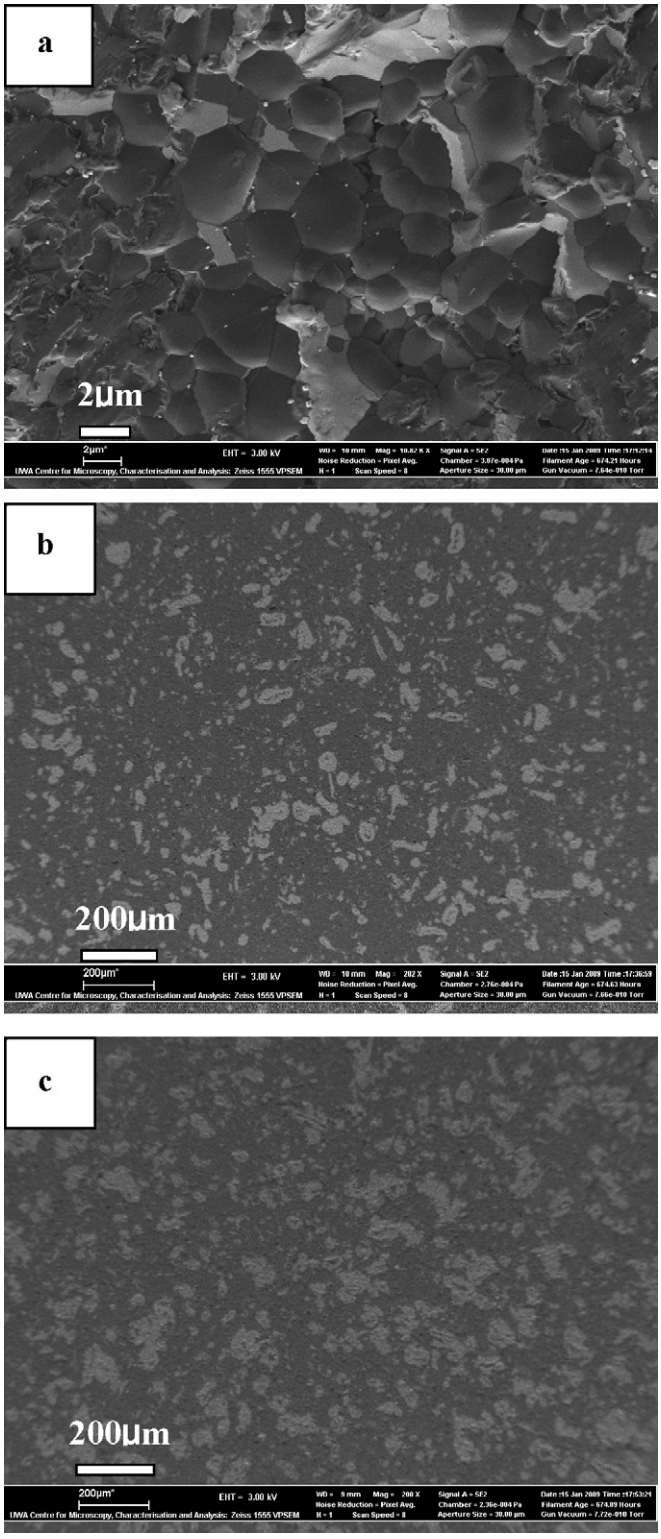

Fig. 5. SEM images of TiAl/B_4C composites after 30 days seawater corrosion: (a) #2 sample; (b) #3 sample; (c) #4 sample.

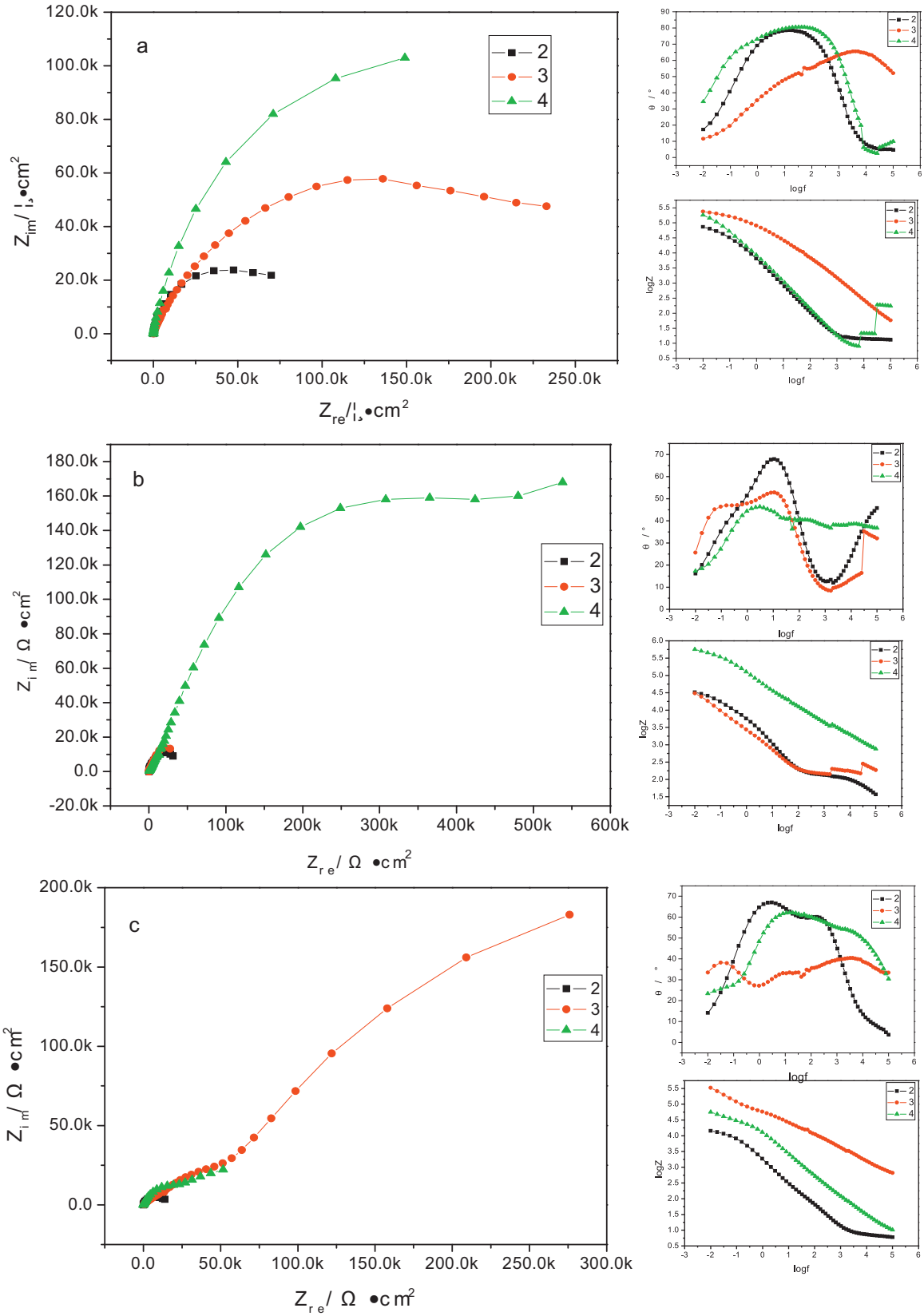

Fig. 6. EIS and Nyquist plots of #2, #3, and #4 samples after (a) 1 day; (b) 15 days; (c) 30 days immersion.

measurements errors are at around 2–5%. The relative density increases while the hardness decreases with increasing the content of Ti and Al. The low-melting TiAl alloy is formed during the sintering procedures. Under a pressure of 20 MPa and a dwell time of 30 min, the liquid TiAl phase can fill-up pore space of ceramics and the residual gas in the ceramic body

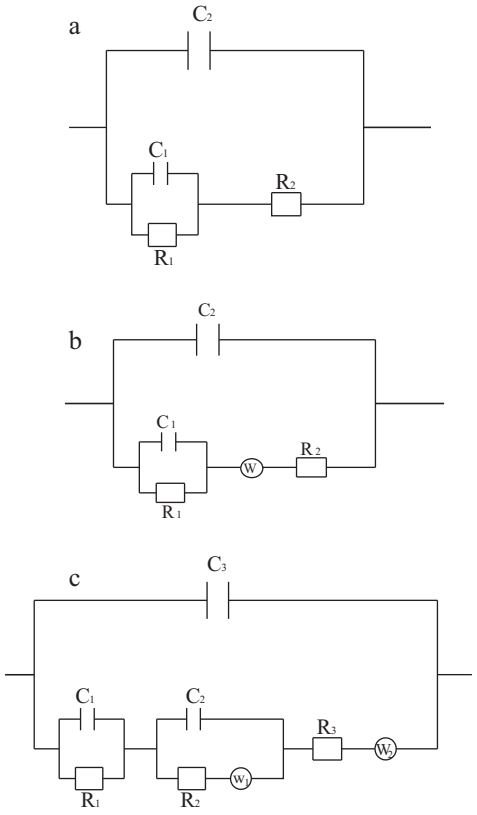

Fig. 7. Equivalent circuits of the studied system over samples (a) #2; (b) #3 (c) #4.

can diffuse or escape, making the composite more compact. As a result, the relative density of the composites is increased. In sample #2, most of the IMC TiAl alloy is staying in between the ceramics, so their surface hardness shows a little drop. When the TiAl alloys agglomerate and cover the composite surface (sample #4), the hardness decreases due to TiAl hardness being lower than for the carbide or boride ceramics.

3.3. Corrosion behavior of TiAl/B_4C series samples

The surface of as fabricated TiAl/B_4C composites corroded in seawater for 30 days is shown in the SEM images of sample #2 (Fig. 5). No serious corrosion happened on these composites. The surfaces are smooth and homogeneous and no pits or holes can be detected.

The corrosion resistance can be estimated by means of electrochemical impedance spectroscopy (EIS). The Nyquist plots obtained for the three samples after 1 day, 15 days, 30 days of immersion in the seawater are presented in Fig. 6. The electrochemical measurement failed for the sample #1 because of its poor electric conductivity due to the low content of TiAl. The impedance spectroscopy is based on the measurement of the response of the electrochemical cell to an alternating potential of small amplitude. Impedance data were analyzed and fitted to circuit parameters using the non-linear least square method in the program EQUIVCRT by Bernard and Boukamp [11]. The electrochemical cell can be modeled as an equivalent circuit with a parallel combination of a double-layer capacitance (Cdl) and charge transfer resistance (Rt) in series with the solution resistance (Rs), which corresponds to the simplest physical situation at an electrode surface. It must be emphasized that there will often exist different model circuits that produce identical impedance responses and the most common circuit type was chosen herein for simplicity (Fig. 7). In a practical electrode system, the impedance spectra are often depressed semicircles with their center below the real axis. The capacitive loops are not perfect semicircles, because the Nyquist plots obtained in the real system represent a general behavior where the double layer on the interface of metal/solution does not behave as a real capacitor. On the metal side, electrons control the charge distribution whereas on the solution side it is controlled by ions. Since ions are much larger than the electrons, the equivalent ions on the metal will occupy quite a large volume on the solution side of the double layer [12]. This phenomenon is known as the dispersing effect [13]. The double-layer not behaving as an ideal capacitor in the presence of the dispersing effect, a constant phase element (i.e., CPE) is often used as a substitute for the capacitor in the equivalent circuit to fit the impedance behavior of the electrical double layer more accurately. The CPE is a special element, whose value is a function of the angular frequency, ω, and whose phase is independent of the frequency. Its admittance and impedance are, respectively, expressed as:

$$Y_{\mathrm{CPE}} = Y_0(\mathrm{j}\omega)^n \tag{1}$$

$$Z_{\mathrm{CPE}} = \frac{1}{Y_0(\mathrm{j}\omega)^{-n}}, \tag{2}$$

where Y_0 is the magnitude of the CPE, ω is the angular frequency and n is the exponential term of the CPE. The CPE may also be used to account for the roughness of the solid electrode, whereby the lower the value of n, the rougher the electrode surface. The reciprocal of the charge-transfer

Table 1
Electrochemical model impedance parameters of samples #2, #3 and #4 immersed in seawater of 30 days.

Sample	R_1	Z_1	n_1	R_2	Z_2	n_2	W
#2	1.44 KΩ	1.00 fF	5.189 μ	14.76 Ω	14.82 μF	0.7477	
#3	46.98 KΩ	9.68 μF	0.977 μ	194.71 Ω	39.001 nF	0.4686	24.36 DW
#4	4.77 Ω	401.00 kF	0.408 μ	7.29 Ω	1.00 pF	0.3215	

Sample	R_3	Z_3	n_3	W_1	W_2
#4	42.94 kΩ	1.281 nF	0.677	8.422 DW	6.293 kDW

resistance, Rt, corresponds to the corrosion rate of a metal in corrosive solutions. A smaller Rt corresponds to a faster corrosion rate. The simulated impedance parameters of Table 1 show that the Rct, Rc, and Rs values recorded for samples in sterile seawater increase rapidly when the proportion of TiAl increased. This emphasizes the fact that the oxide film plays an important role in improving the corrosion resistance of the sample. With the increase in the content of TiAl, the oxide film can form more easily and cover more consistently. The constant phase elements (CPEs, Cdl) with their *n* values close to 1.0 represent double layer capacitors with some pores on the surface of samples. It is noteworthy that Rct for the series samples decreased with the increase of TiAl, confirming the protective nature of oxides formed on the surface during immersion. The diffusion tail observation on the spectrum is most likely due to a previously established mechanism of Al^{3+} diffusion through a surface film (a process which is rate-limiting when sample is exposed to neutral water).

4. Conclusions

TiAl/B_4C composites marine materials have been successfully fabricated from the Ti–Al–B_4C system by combining high energy ball milling and hot press sintering process. The composites consist of TiAl, TiC, TiB_2, and B_4C. When the total amount of Ti and Al is 20 wt.%, a sandwich structure results with IMC TiAl alloy as a core. Further increasing Ti and Al content to 40 wt.%, the sandwich structure disappears, the TiAl alloy agglomerates and covers on the surface of the carbide and boride ceramic surfaces. The density increases while the hardness decreases with the increase of the Ti and Al in the composite. The maximum value of bending strength and fracture toughness of the composites is 437.3 MPa and 4.85 MPa $m^{1/2}$, respectively. The potentiodynamic polarization measurements and electrochemical impedance spectroscopy results indicate that such composites are novel anticorrosive materials in seawater.

Acknowledgement

We thank the financial support from the China Scholarship Council (CSC [2008] 3019).

References

[1] D. Jollivet, Specific and genetic diversity at deep-sea hydrothermal vents: an overview, Biodiversity and Conservation 5 (1996) 1619–1653.
[2] R.Z. Lutz, M.J. Kennish, Ecology of deep-sea hydrothermal vent communities, Reviews of Geophysics 31 (1993) 211–241.
[3] E. Aragon, J. Woillez, C. Perice, F. Tabaries, M. Sitz, Development of novel multilayer materials for impact applications, Materials and Design 30 (2009) 1548–1555.
[4] J.X. Deng, J.L. Sun, Microstructure and mechanical properties of hot-pressed B_4C/TiC/Mo ceramic composites, Ceramics International 35 (2009) 771–778.
[5] S. Mondal, A.K. Banthia, Low-temperature synthetic route for boron carbide, Journal of the European Ceramic Society 25 (2005) 287–291.
[6] F. Thévenot, Boron carbide—a comprehensive review, Journal of the European Ceramic Society 6 (1990) 205–225.
[7] V.A. Lavrenko, A.D. Panasyuk, S.A. Firstov, S.B. Prima, V.O. Kochubei, V.M. Adeev, Corrosion of titanium–aluminum intermetallides. 2. Electrolytic oxidation of γ-TiAl, $TiAl_3$, and α_2-Ti_3Al in sea water, Powder Metallurgy and Metal Ceramics 42 (2003) 291–296.
[8] B.L. Zou, P. Shen, Q.C. Jiang, Dependence of the SHS reaction behavior and product on B_4C particle size in Al–Ti–B_4C and Al–TiO_2–B_4C systems, Materials Research Bulletin 44 (2009) 499–504.
[9] H.Y. Wang, Q.C. jiang, Y.Q. Zhao, F. Zhao, Fabrication of TiB_2 and TiB_2–TiC particulates reinforced magnesium matrix composites, Materials Science and Engineering A 372 (2004) 109–114.
[10] Q.C. Jiang, X.L. Li, H.Y. Wang, Fabrication of TiC particulate reinforced magnesium matrix composites, Scripta Materialia 48 (2003) 713–717.
[11] A. Bernard, Boukamp, Electrochemical impedance spectroscopy in solid state ionics: recent advances, Solid State Ionics 169 (2004) 65–73.
[12] M. Ozcan, M. Dehri, Erbil, Organic sulphur-containing compounds as corrosion inhibitors for mild steel in acidic media: correlation between inhibition efficiency and chemical structure, Applied Surface Science 236 (2004) 155–164.
[13] J.E. Weber, Dispersion effect on buoyancy-driven convection in stratified flows through porous media, Journal of Hydrology 25 (1975) 59–70.